Diffraction-assisted micropatterning of silicon surfaces by ns-laser irradiation

E. Haro-Poniatowski, C. Acosta-Zepeda, G. Mecalco, J. L. Hernández-Pozos, N. Batina, I. Morales-Reyes, and J. Bonse

Citation: Journal of Applied Physics **115**, 224309 (2014); doi: 10.1063/1.4882660
View online: http://dx.doi.org/10.1063/1.4882660
View Table of Contents: http://scitation.aip.org/content/aip/journal/jap/115/22?ver=pdfcov
Published by the AIP Publishing

Diffraction-assisted micropatterning of silicon surfaces by ns-laser irradiation

E. Haro-Poniatowski,[1,a)] C. Acosta-Zepeda,[1] G. Mecalco,[1] J. L. Hernández-Pozos,[1] N. Batina,[2] I. Morales-Reyes,[2] and J. Bonse[3]
[1]*Departamento de Física, Universidad Autónoma Metropolitana Iztapalapa, Av. San Rafael Atlixco No. 186, Col. Vicentina, C.P. 09340 México D. F., Mexico*
[2]*Departamento de Química, Universidad Autónoma Metropolitana Iztapalapa, Av. San Rafael Atlixco No. 186, Col. Vicentina, C.P. 09340 México D. F., Mexico*
[3]*BAM Bundesanstalt für Materialforschung und-prüfung, Unter den Eichen 87, D-12205 Berlin, Germany*

(Received 14 April 2014; accepted 29 May 2014; published online 13 June 2014)

Single-pulse (532 nm, 8 ns) micropatterning of silicon with nanometric surface modulation is demonstrated by irradiating through a diffracting pinhole. The irradiation results obtained at fluences above the melting threshold are characterized by scanning electron and scanning force microscopy and reveal a good agreement with Fresnel diffraction theory. The physical mechanism is identified and discussed on basis of both thermocapillary and chemicapillary induced material transport during the molten state of the surface. © *2014 AIP Publishing LLC*. [http://dx.doi.org/10.1063/1.4882660]

I. INTRODUCTION

Pulsed laser irradiation of surfaces can have very different effects depending on several parameters such as pulse duration, wavelength, and energy density among others. The effect of the laser irradiation can range from material removal (ablation) to annealing of crystalline defects or other non-ablative processes giving rise to topographic features with various surface morphologies at the nano/micro scale. The corresponding applications include laser texturing,[1] laser annealing,[2] laser scribing,[3] laser surface engineering,[4] laser-induced periodic surface structures[5] (LIPSS, ripples), and recently laser-induced plasmonic structures.[6,7]

One of the first applications of nanosecond (ns) laser technology arising in the mid-seventies was laser annealing of semiconductors and in particular silicon.[2] During the last decades, ns-laser technology has reached a mature state and is nowadays an integral part of various industrial materials processing strategies. In particular, "laser texturing." Laser surface texturing (LST) at the microscale was first employed to improve the tribological surface characteristics of materials in the 1990s.[1] Additionally, it was demonstrated that laser-induced patterned microstructures on the surface of the materials can improve their properties such as wear rates and lubrication lifetime. Lasers provide excellent control of the surface microstructure compared to other surface etching processes.[8] It is important to point out that laser texturing is not always based on material removal as it is the case in laser ablation, in the case of laser texturing a hydrodynamic redistribution of the molten region occurs.[9] Finally, an additional important application of laser marking (patterning) is in semiconductor manufacturing processes for the identification (ID) of individual wafers.[10]

Extending these results to the nanometer scale implies circumventing the diffraction limit arising from the use of conventional optical systems. One solution is the development and use of near field technologies. As an example, arrays of self assembled nano-/micro-sized spheres on a surface have been employed. Patterning can be achieved by two different processes: direct irradiation of the surface through the holes of the array giving rise to triangular shapes and electromagnetic field enhancement at the bottom of each sphere.[11,12]

In this work, we take benefit from optical diffraction effects to realize more complex surface structures reaching micrometer precision on the lateral scale. The obtained diffraction pattern is imprinted on the surface of the Si wafer, resulting in surface displacements of the order of tens of nanometers only in the vertical direction. In the high intensity regions, which in this case are rings, the silicon melts and moves towards the low intensity regions generating a surface depression (valley). In the low intensity regions, a ring-shaped protrusion is formed. These matter transport processes arise from the Marangoni effect; thermocapillary and chemicapillary forces are acting on the silicon melt. The observed optical patterning is explained with Fresnel diffraction theory and a good agreement between theory and experiment is obtained. This diffraction-based processing technique[13] opens up the possibility to influence the patterning effects through the spatial parameters characterizing the mask and its distance to the sample.

II. EXPERIMENTAL DETAILS

Figure 1 shows the experimental set-up for the laser irradiation experiments of commercial single-crystalline silicon wafers (WRS Materials, San José, USA, ⟨100⟩ crystal orientation, *n*-doped (phosphorous), wafer thickness 350–400 μm). It is based on the diffraction pattern generated by a single laser pulse (532 nm, 8 ns, beam diameter 3 mm), emitted from a frequency-doubled Nd:YAG laser (Continuum-Minilite), at a distance d typically a few hundreds of micrometers behind a circular diffracting mask (a pinhole with a diameter of $a = 70\,\mu$m) which is illuminated at a distance of $Z \sim 60$ mm through a $f = 70$ mm focal length lens. In this irradiation geometry, the optical transmission of

[a)]Author to whom correspondence should be addressed. Electronic mail: haro@xanum.uam.mx

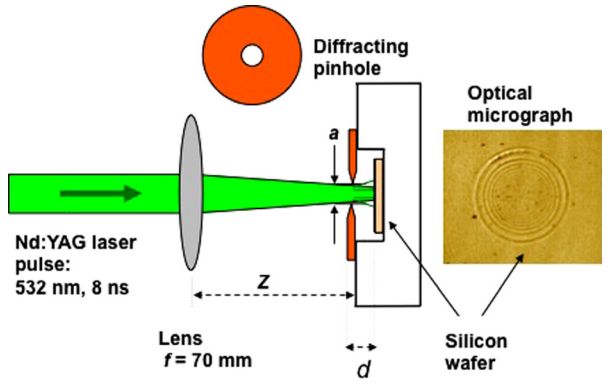

FIG. 1. Experimental setup for diffraction-assisted micropatterning of the silicon wafer. Typical distances: Z (from lens to pinhole) = 60 mm, a (pinhole diameter = 70 μm), d (sample-mask distance ~ 100–300 μm), and f (focal length of the lens = 70 mm).

the focused laser beam through the pinhole aperture is approximately $T = 0.27$.

For suitable laser pulse energies (E_P), the structured light illumination field resulting from the diffraction at the pinhole locally modifies the material and leads to an annular ring pattern imprinted in the surface topography as shown in Fig. 1. This technique has been referred to as *diffraction-assisted method* (DAM)[14] and was successfully used to locally modify the size and morphology of nanostructured thin films.[13,15] All irradiation were performed in air. Prior to irradiation, the silicon wafers were cleaned using ethanol.

The laser irradiated surface regions were characterized by optical microscopy (OM), scanning electron microscopy (SEM; JEOL7600F), and scanning force microscopy (SFM; Digital Instruments, Nanoscope III) operated in tapping mode at line scan rates below 1 Hz.

III. RESULTS

A. Diffraction-assisted micropatterning and surface characterization

Figure 2 presents the comparison of a SEM images and the corresponding scanning force microscopic images of two surface spots irradiated with a single ns-laser pulse ($E_P = 1.0$ mJ) at two different sample-mask distances $d = 150\ \mu$m and 250 μm ($\pm 25\ \mu$m), respectively.

Several concentric rings are clearly distinguishable in all SEM/SFM micrographs [(a) and (d)]. The SFM cross-sectional profile along the dashed horizontal lines [see Fig. 2(d)] reveals very shallow surface depressions and protrusions of less than ± 15 nm in both cases [see Fig. 2(c)].

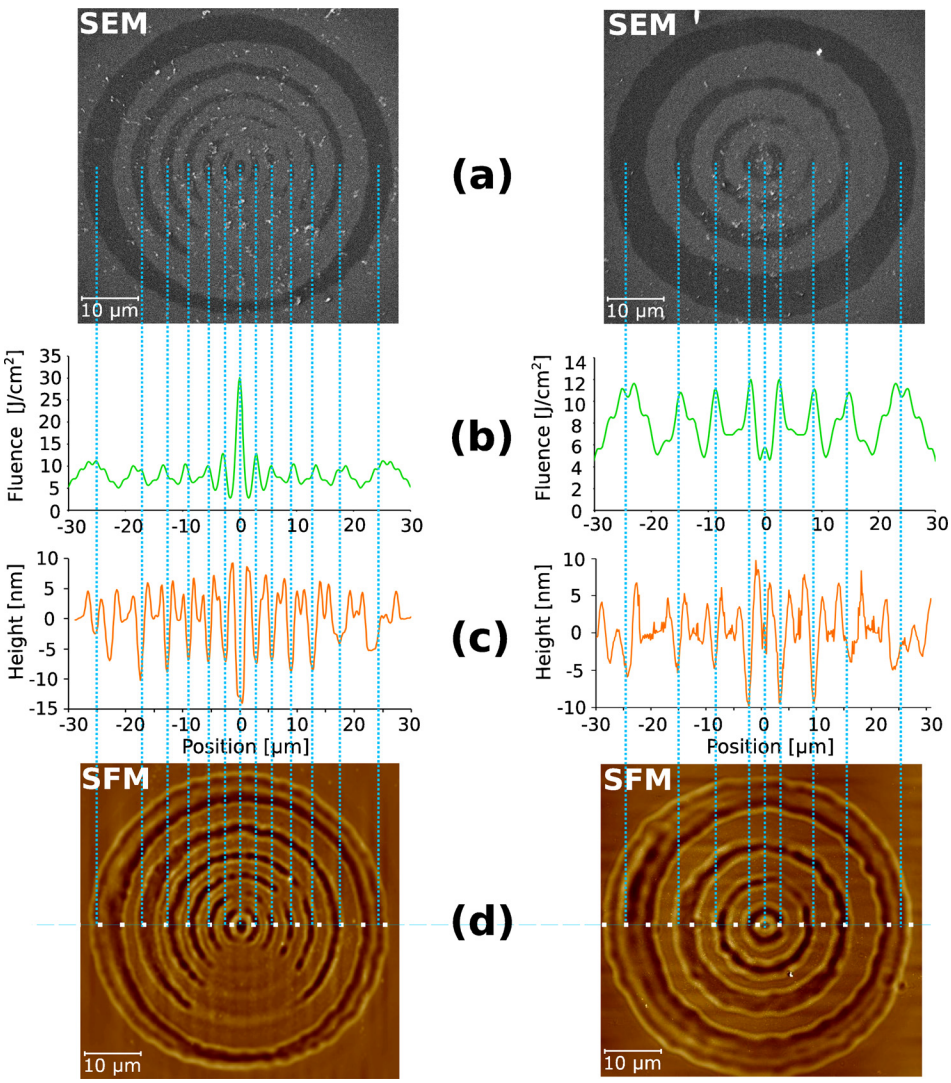

FIG. 2. SEM micrographs (a) and SFM topography images (d) of two DAM-micropatterned spots on a silicon wafer surface ($E_P = 1.0$ mJ) irradiated at two different mask to sample distances $d = 150\ \mu$m $\pm$ 25 μm (left column) and $d = 250\ \mu$m $\pm$ 25 μm (right column). The corresponding calculated fluence and height profiles [along the dashed white lines in (d)] are shown in (b) and (c). Note the different vertical scales used in (b) and (c) for both columns.

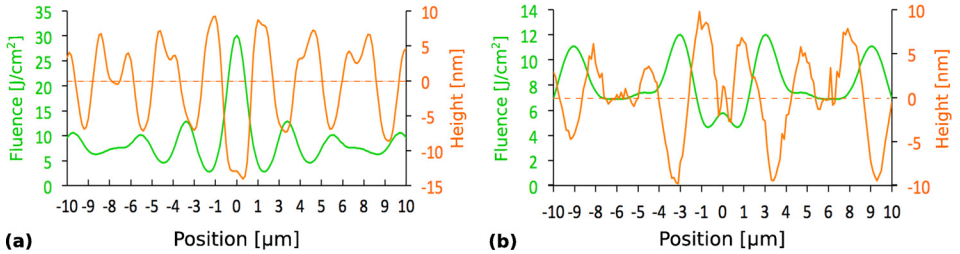

FIG. 3. Expanded view of the fluence (left vertical scale) and height (right vertical scale) spatial profiles (as previously shown in Fig. 2). (a) $d = 150\,\mu\text{m} \pm 25\,\mu\text{m}$, (b) $d = 250\,\mu\text{m} \pm 25\,\mu\text{m}$.

Regions appearing dark in the SEM micrographs are associated with shallow surface depressions of the SFM topography [compare Figs. 2(a) and 2(c)]. The separation width and depth of the rings both vary in the radial direction. These results are in close correspondence with those reported before[13] on laser-irradiated nanostructured silver thin films.

In order to analyze the obtained experimental results a Fresnel diffraction model for a circular pinhole was used. The analysis is equivalent to the one presented in Ref. 13 and is resumed in Sec. III B. The result of the radial irradiance profile is presented by the green curves shown in Fig. 2(b). A close correspondence between the position of the peaks and the patterned surface is observed. An expanded view of the cross-sectional irradiance and the height profiles is given in Figs. 3(a) and 3(b) corresponding to the two micropatterned spots described before.

B. Fresnel diffraction theory

For some simple cases, such as the patterning of silver quasipercolated thin films diffracted by a razor edge or a single slit was already shown that the experimental results can be described using Fresnel diffraction theory.[16] The case of circular apertures is mathematically more complex.[15,17] In the present case, the same formalism can be used. To calculate the spatial intensity distribution produced by the diffraction of a circular aperture, we consider an observation point P at the plane of the sample. The sample is located at a distance Z_0 from the mask with a circular aperture with a diameter a.

The intensity I is given by

$$I = \left(\frac{a^2\pi}{\lambda Z_0}\right)^2 (C^2(u,v) + S^2(u,v)), \tag{1}$$

with

$$C(u,v) = \frac{2}{u}\sin\frac{v^2}{2u} + \frac{\sin\frac{1}{2}u}{\frac{1}{2}u}V_0(u,v) - \frac{\cos\frac{1}{2}u}{\frac{1}{2}u}V_1(u,v),$$

$$S(u,v) = \frac{2}{u}\cos\frac{v^2}{2u} - \frac{\cos\frac{1}{2}u}{\frac{1}{2}u}V_0(u,v) - \frac{\sin\frac{1}{2}u}{\frac{1}{2}u}V_1(u,v),$$

$V_0(u,v)$ and $V_1(u,v)$ are Lommel functions given by

$$V_n(u,v) = \sum_{s=0}^{\infty}(-1)^s\left(\frac{v}{u}\right)^{n+2s}J_{n+2s}(v),$$

where $J_n(v)$ is the Bessel function and the dependence on the spatial coordinates x, y is given by $u = \frac{ka^2}{z_0}$, $v = \frac{kar}{z_0}$, with $r = \sqrt{x^2+y^2}$.

The theoretical diffraction intensity profile $I(r)$ resulting from the mask with a hole is calculated by solving Eq. (1). As the intensity I and the laser fluence ϕ are linearly related ($\phi = \text{A} \times I$), the proportionality constant (A) was calculated by integrating $\phi(x,y)$ over the sample plane and subsequent normalization with the transmitted laser pulse energy.

$$E_{tr} = T \cdot E_P = \int_{-\infty}^{+\infty}\int_{-\infty}^{+\infty}\phi(x,y)\cdot dx\cdot dy = 2\pi\cdot A\int_0^{\infty} I(r)\cdot r\cdot dr. \tag{2}$$

For the given case ($T = 0.27$, $E_P = 1.0$ mJ), the corresponding calculated radial fluence distributions and are presented in Figs. 2(b) and 3 (green lines) as a function of the horizontal position in the surface plane of the sample. Using the measured experimental parameters (laser wavelength $\lambda = 532$ nm, distance from the mask to the sample $d = 150\,\mu\text{m} \pm 25\,\mu\text{m}$ in one case and $d = 250\,\mu\text{m} \pm 25\,\mu\text{m}$ in the second case, pinhole diameter $a = 70\,\mu\text{m}$), the oscillations of the diffracted patterns match well the spacing between the induced morphological rings. It is important to note that in our experimental setup the distance d between pinhole and mask and the parallelism between the sample and the mask surfaces were difficult to control precisely. As consequence of the diffraction affected by this, the ring pattern imprinted to the silicon surface is not complete (see Fig. 2, left column). Hence, this distance $d = Z_0$ was considered as an adjustable parameter allowing a variation of up to 15% in the Fresnel diffraction calculations. The best agreement (position of the diffracted intensity peaks and their corresponding width) between the calculated diffraction pattern and our experimental surface morphologies were obtained for $Z_0 = 173\,\mu\text{m}$ and $Z_0 = 250\,\mu\text{m}$, respectively (Fig. 2, left and right). Both values of Z_0 agree within the experimental uncertainty of $\pm 25\,\mu\text{m}$ with the sample-mask distances d specified for Figs. 2 and 3.

IV. DISCUSSION

The surface depressions are formed in the regions of highest fluence [marked by vertical dotted lines in Fig. 2], suggesting that ablation or melt flows are responsible for their formation. The importance of melt flows is further supported by the fact that each depression is always bordered by protrusions along with the observation of an almost unaltered surface between the depressions. From the expanded surface and fluence profiles, shown in Fig. 3, one can find additional clues supporting that melt flow and subsequent solidification

are responsible for the resulting morphology. Consider for instance the central region in Fig. 3(b) where the fluence distribution shows a local maximum exactly at the center position (0 μm). The corresponding surface height profile shows a small protrusion instead of a depression. This protrusion is very likely due to the melt flow from the first two nearest neighbor peaks to the central one in the spatial fluence distribution.

Moreover, in the direct comparison between fluence and surface height profiles, one can see that the ratio of both entities is not constant—particularly in Fig. 3(a), where the central fluence (factor 2–3 enhanced fluence) does *not* lead to a 2–3 times deeper crater (just a factor of ~1–2), indicating a weak dependence of the maxima of the surface height profile on the laser fluence.

The calculated fluences allow a comparison to the thresholds of phase transitions reported in the literature for irradiation of silicon wafers by 532-nm ns-laser pulses. Schwarz-Selinger *et al.*[9] reported for 1-ns laser pulses a melting threshold of $\phi_{melt} = 0.21\,J/cm^2$ and a threshold of $\phi_{deoxi} \sim 0.6\,J/cm^2$ for the break-up of the native oxide layer. That melting threshold is close to the value of $\phi_{melt} = 0.38\,J/cm^2$ found earlier by Lowndes *et al.*[18] for 18-ns laser pulses in time resolved reflectivity measurements. The onset of ablation (particle emission) was reported by van Brug *et al.*[19] for 15-ns laser pulses at fluences around $\phi_{abl} \sim 3\,J/cm^2$. These threshold values confirm that the melting threshold is exceeded in our experiments here. The literature value of the ablation threshold of $3\,J/cm^2$ would also suggest that ablation occurs in both micropatterned spots shown in Figs. 2 and 3. Evaluating for these two irradiation spots the topographic volume above and below the original surface plane reveals that these two values are almost identical (for each of the spot). Hence, transient melt flows dominate the surface structuring process and ablation is negligible here. The fact that the calculated fluences are exceeding the literature values of the ablation threshold here might arise from the fact that the fluence normalization procedure using Eq. (2) crucially depends on the radial intensity profiles.[20] However, the experimental proof of material displacement without significant removal of silicon from SFM clearly underlines that the importance of melt flows and that their temporal dynamics must be analyzed in more detail here.

The melt displacements are either caused by thermocapillary flows (Marangoni effect)[21] or can be triggered by a pressure locally induced to the molten surface by ablating material. The Marangoni effect has been investigated and modelled in nanosphere-enhanced laser patterning of silicon.[11] Two distinct components are responsible for the Marangoni flows. The first is thermocapillarity (associated to a local temperature gradient) and the second one is chemicapillarity (associated with local compositional gradient). The local thermal gradient is induced by the spatial laser beam intensity profile. This is initially of Gaussian shape and then transferred upon diffraction at the circular pinhole into a more complex diffraction pattern. The compositional gradient may originate from the native oxide layer at the surface of the Si wafer. When the laser fluence is large enough to activate both processes, the thermocapillary one moves the material outwards from the hottest regions towards the colder edges. In contrast, the chemicapillary effect would move the molten materials inward towards the center.[11] The chemicapillarity is triggered if the laser intensity/fluence is high enough to evaporate the surfactant (the native oxide layer). This effect is responsible for the central bump or peak in the irradiated area in Ref. 11 but it is not observed in our case.

These two forms of capillarity have been investigated in detail for irradiation with a spatially Gaussian beam profile and are responsible for two experimentally observed morphologies in the surface of Ni-P magnetic disks substrates using a single ns-pulse of a Nd:YLF laser (1047 nm, 50 ns).[22,23] Depending on the energy of the irradiation pulse, one can generate a "bowl type" surface deformation having only the rim protruding above the surface (for low energies as in our case) or a "sombrero" like surface profile (with the formation of a peak in the center of the irradiated spot) if the irradiation energy is high enough. These effects also have been reported for silicon surfaces irradiated by a Gaussian beam.[9,21]

The previously presented and discussed results strongly suggest that the surface height profiles observed in Figs. 2 and 3 are caused by Marangoni melt flows generating the bowl-type surface morphologies in the vicinity of each local interference maximum. This hypothesis was further tested based on an estimation of the time which is required to generate such surface deformations compared to the typical melt durations observed for ns-laser irradiation of silicon. According to Ben-Yakar and coworkers[24] the characteristic time τ_M for Marangoni melt flow can be estimated as

$$\tau_M = \frac{\eta L^2}{|\gamma_T| T_m h_0}, \tag{3}$$

where η is the dynamic viscosity of the melt, L is the radial flow distance, h_0 represents an average melt depth, and T_m the melting temperature of the silicon (1690 K). $|\gamma_T| = |d\gamma/dT|$ is the absolute value of the temperature coefficient of the surface tension γ. Assuming $L = 3\,\mu m$ as a typical distance to be bridged between adjacent interference maxima (caused by Fresnel diffraction, see Fig. 3) along with an average melt depth of $h_0 \sim 750\,nm$ (close to the optical penetration depth of 532 nm radiation in silicon) and taking the material parameters of molten silicon[25] $\eta = 0.9 \times 10^{-3}$ N s/m^2, $\gamma_T = -0.28 \times 10^{-3}$ N/(m K) into consideration, a characteristic time for Marangoni flow of $\tau_M \sim 22\,ns$ is estimated here using Eq. (3). This value is approximately twice the pulse duration (8 ns). It is shorter than the melt duration (lifetime of the melt) experimentally observed upon ns-laser irradiation of silicon at 532 nm wavelength, featuring values starting from a few tens of nanoseconds at fluences very close to the melting threshold up to melt durations of ~1 μs at fluences approaching the ablation theshold.[26] Moreover, for the ns-laser pulse durations the absorbed optical energy spreads already

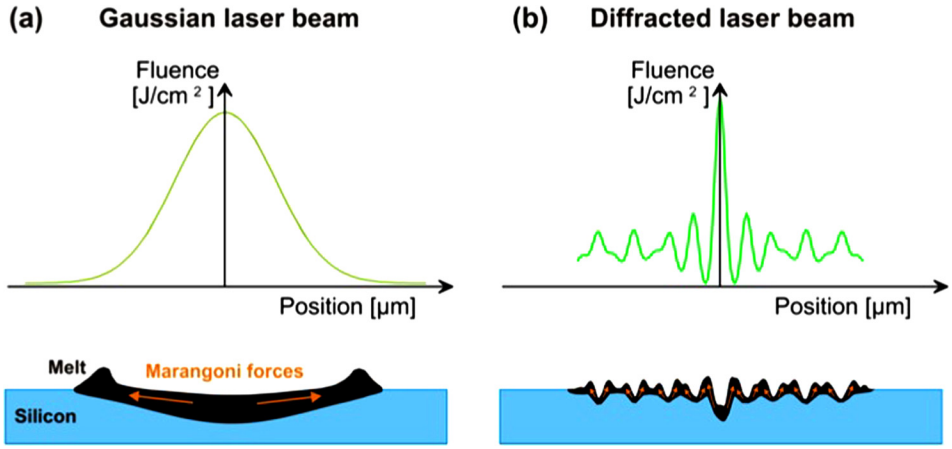

FIG. 4. Scheme of the thermocapillary irradiation effects induced on a silicon wafer surface by a Gaussian laser beam (a) and laser beam diffracted at a circular aperture (b). In both cases, the fluence is sufficient to melt the silicon surface locally (black regions). The arrows indicate the thermocapillary forces due to the Marangoni effect.

during the laser pulse into the surrounding silicon, resulting in a characteristic heat diffusion length of typically a few micrometers.[21] This effect can increase the average melt depth h_0 and, according to Eq. (3), will further decrease the characteristic time required for Marangoni melt flows. Hence, the proposed Marangoni melt flow scenario appears reasonable here as there is enough time for the molten surface to evolve into the observed surface morphologies.

The summarizing scheme shown in Figure 4 compares the laser processing of a silicon wafer surface during the irradiation with a Gaussian laser beam [Fig. 4(a)] with that of a Fresnel-diffracted Gaussian laser beam [Fig. 4(b)]. The melt layer transiently formed upon the irradiation is sketched in black, while the local thermocapillary forces resulting from the Marangoni effect are indicated as orange arrows in both parts of the figure. For irradiation with a Gaussian beam, the thermocapillary forces are always directed outwards, resulting in a rim around the irradiated spot. In contrast, a diffracted laser beam induces both, inwards and outwards directed forces, which are finally leading to annular rims surrounding each surface depression.

V. CONCLUSIONS

Single shot laser (532 nm, 8 ns) micropatterning of a silicon wafer through a diffractive circular mask (pinhole) was demonstrated. For suitable laser pulse energies, the structured light illumination field resulting from the diffraction locally modifies the material and leads to a very shallow annular ring pattern imprinted in the surface topography. The results were compared to the Fresnel diffraction theory and revealed that melting occurs in the regions of the highest intensities, finally triggering local melt displacements (height modulation $< \pm 15$ nm after surface solidification).

[1]I. Etsion, "State of the art in laser surface texturing," J. Tribol. **127**, 248–253 (2005).
[2]E. I. Shtyrkov, I. B. Khaibullin, M. M. Zaripov, M. F. Galyatudinov, and R. M. Bayazitov, "Local laser annealing of implantation doped semiconductor layers," Sov. Phys. Semicond. **9**, 1309–1310 (1975).
[3]J. Bovatsek, A. Tamhankar, R. S. Patel, N. M. Bulgakova, and J. Bonse, "Thin film removal mechanisms in ns-laser processing of photovoltaic materials," Thin Solid Films **518**, 2897–2904 (2010).
[4]J. Th. M. De Hosson, V. Ocelík, U. O. B. de Oliveira, and D. I. Vainchtein, "Fundamental and applied aspects of laser surface engineering," Int. J. Mater. Res. **100**, 1343–1360 (2009).
[5]J. Bonse, J. Krüger, S. Höhm, and A. Rosenfeld, "Femtosecond laser-induced periodic surface structures," J. Laser Appl. **24**, 042006 (2012).
[6]G. Obara, N. Maeda, T. Miyanishi, M. Terakawa, N. N. Nedyalkov, and M. Obara, "Plasmonic and Mie scattering control of far-field interference for regular ripple formation on various material substrates," Opt. Express **19**, 19093–19101 (2011).
[7]R. J. Peláez, C. N. Afonso, J. Bulír, M. Novotny, J. Lančok, and K. Piksová, "2D plasmonic and diffractive structures with sharp features by UV laser patterning," Nanotechnology **24**, 095301 (2013).
[8]M. Duarte, A. Lasagni, R. Giovanelli, J. Narciso, E. Louis, and F. Mücklich, "Increasing lubricant film lifetime by grooving periodical patterns using laser interference metallurgy," Adv. Eng. Mater. **10**, 554–558 (2008).
[9]T. Schwarz-Selinger, D. G. Cahill, S. C. Chen, S. G. Moon, and C. P. Grigoropoulos, "Micron-scale modifications of Si surface morphology by pulsed-laser texturing," Phys. Rev. B **64**, 155323 (2001).
[10]T. Chiba, R. Komura, and A. Mori, "Formation of micropeak array on a silicon wafer," Jpn. J. Appl. Phys., Part 1 **39**, 4803–4810 (2000).
[11]Y. Lu, S. Theppakuttai, and S. C. Chen, "Marangoni effect in nanosphere-enhanced laser nanopatterning of silicon," Appl. Phys. Lett. **82**, 4143–4145 (2003).
[12]A. Kolloch, T. Gedhauser, K. Ueno, H. Misawa, J. Boneberg, A. Plech, and P. Leiderer, "Femtosecond and picosecond near field ablation of gold nanotriangles: nanostructuring and nanomelting," Appl. Phys. A: Mater. Sci. Process. **104**, 793–799 (2011).
[13]E. Haro-Poniatowski, J. C. Alonso-Huitrón, C. Acosta-Zepeda, M. C. Acosta-García, and N. Batina, "Laser-induced micron and submicron ordering effects in quasi-percolated nanostructured silver thin films," Nanotechnology **20**, 355304 (2009).
[14]O. Van Overshelde and M. Wautelet, "Diffraction-aided laser-induced microstructuring of thin TiO_2 films on glass," Appl. Phys. Lett. **89**, 161114 (2006).
[15]J. C. Alonso-Huitrón, E. Haro-Poniatowski, C. Acosta-Zepeda, N. Batina, M. C. Acosta-García, and P. Castillo-Ocampo, "UV-laser induced modifications through a single slit on quasi-percolated silver nanostructured films," Radiat. Eff. Defects Solids **164**, 438–442 (2009).
[16]E. Haro-Poniatowski, J. P. Lacharme, C. Ricolleau, and E. Fort, "Patterning of nanostructured thin films by structured light field illumination," Appl. Phys. Lett. **87**, 143103 (2005).
[17]M. Born and E. Wolf, *Principles of Optics*, 7th ed. (Cambridge University Press, Cambridge, 1999), Chap. VIII, pp. 484–492.
[18]D. H. Lowndes, R. F. Wood, and R. D. Westbrook, "Pulsed neodymium: yttrium aluminum garnet laser (532 nm) melting of crystalline silicon: Experiment and theory," Appl. Phys. Lett. **43**, 258–260 (1983).

[19]H. van Brug, K. Murakami, F. Bijerk, and M. J. van der Wiel, "Time-resolved x-ray monitoring of laser ablation and plasma formation from silicon," J. Appl. Phys. **60**, 3438–3443 (1986).
[20]While the position of the intensity peaks is well reproduced by the Fresnel diffraction theory, deviations to the experiment may be expected in the modulation depths of the calculated intensity peaks, as the experiment realized here lies in between the two limiting cases of Fresnel and Fraunhofer diffraction.
[21]D. Bäuerle, *Laser Processing and Chemistry*, 4th ed. (Springer-Verlag, Berlin, 2011), Chap. 10.
[22]T. D. Bennett, D. J. Krajnovich, C. P. Grigoropoulos, P. Baumgart, and A. C. Tam, "Marangoni mechanism in pulsed laser texturing of magnetic disk substrates," J. Heat Transfer **119**, 589–596 (1997).
[23]S. C. Chen, D. G. Cahill, and C. P. Grigoropoulos, "Melting and surface deformation in pulsed surface micromodification of Ni-P disks," J. Heat Transfer **122**, 107–112 (2000).
[24]A. Ben-Yakar, A. Harkin, J. Ashmore, R. L. Byer, and H. A. Stone, "Thermal and fluid processes of a thin melt zone during femtosecond laser ablation of glass: the formation of rims by single laser pulses," J. Phys. D: Appl. Phys. **40**, 1447–1459 (2007).
[25]S. Nakamura and T. Hibiya, "Thermophysical properties data on molten semiconductors," Int. J. Thermophys. **13**, 1061–1084 (1992).
[26]D. H. Auston, J. A. Golovchenko, A. L. Simons, C. M. Surko, and T. N. C. Venkatesan, "Dynamics of Q-switched laser annealing," Appl. Phys. Lett. **34**, 777–779 (1979).